Biomaterials 270 (2021) 120683

Contents lists available at ScienceDirect

Biomaterials

journal homepage: www.elsevier.com/locate/biomaterials

A multi-niche microvascularized human bone marrow (hBM) on-a-chip elucidates key roles of the endosteal niche in hBM physiology

Michael R. Nelson [a,1], Delta Ghoshal [a,1], Joscelyn C. Mejías [a], David Frey Rubio [a], Emily Keith [a], Krishnendu Roy [a,b,*]

[a] The Wallace H. Coulter Department of Biomedical Engineering, Georgia Institute of Technology and Emory University, Atlanta, GA, 30332, USA
[b] The Parker H. Petit Institute for Bioengineering & Bioscience, Georgia Institute of Technology, Atlanta, GA, 30332, USA

ARTICLE INFO

Keywords:
Microfluidic chip
Bone marrow niche
Hematopoietic stem cells
Radiation

ABSTRACT

The human bone marrow (hBM) is a complex organ critical for hematopoietic and immune homeostasis, and where many cancers metastasize. Understanding the fundamental biology of the hBM in health and diseases remain difficult due to complexity of studying or manipulating the BM in humans. Accurate biomaterial-based *in vitro* models of the hBM microenvironment are critical to further our understanding of the BM-niche and advancing new clinical interventions. Here we report a unique, 96-well format, microfluidic hBM-on-a-chip that incorporates the endosteal, central marrow, and perivascular niches of the human BM. Osteogenic differentiation of donor human mesenchymal stromal cells (MSCs) produced robust mineralization on the bottom surface ("bone-like endosteal layer") of the device, and subsequent seeding of human endothelial cells and MSCs in a fibrin-collagen hydrogel network ("central marrow") on the top created an interconnected 3D microvascular network ("perivascular niche"). The 96-well format allows eight independent "chips" to be studied in one plate, thereby increasing throughput and reproducibility. We show that this complex, multi-niche microtissue accurately mimics hBM composition and microphysiology, while providing key insights on hematopoietic progenitor dynamics. Presence of the endosteal niche decreased the proliferation and increased maintenance of $CD34^+$ hematopoietic stem cells (HSCs). Upon exposure to radiation, HSCs in the hBM-chips containing endosteal niches were less frequently apoptotic, suggesting a potentially radio-protective role of the osteoblast surface. Our methods and results provide a broad platform for creating complex, multi-niche, high-throughput microphysiological (MPS) systems. Specifically, this hBM-on-a-chip opens new opportunities in human bone marrow research and therapeutics development, and can be used to better understand normal and impaired hematopoiesis, and various hBM pathologies, including cancer and BM failures.

1. Introduction

Hematopoietic stem cells (HSCs) reside and self-renew in the bone marrow (BM) throughout adulthood, where multipotency is maintained and hematopoietic progenitor cells (HPCs) differentiate to maintain homeostasis [1]. The microenvironment that maintains HSC potency and regulates differentiation of HPCs, i.e. the HSC niche, is characterized by BM stromal cells, extracellular matrix (ECM), and biochemical and physical signals [2–5]. The HSC niche can be disrupted naturally with age, with radiation or chemotherapies, or by primary and metastatic malignancies in the BM, and also through the mobilization of HSCs for apheresis. Novel, human, and potentially patient specific, models of this microenvironment are critical to advancing our understanding of the BM niche, developing new BM directed therapeutics, and evaluating the effects and predicting the success (or failure) of clinical interventions [6].

Our understanding of the structure, composition, and function of the BM microenvironment has been changing over the last two decades. Early research had indicated that HSCs resided in a hypoxic, endosteal niche, where their potency was maintained [7,8]. However, more recent findings have argued that multi-potent HSCs maybe perivascular and exist in a niche maintained by endothelial cells and perivascular stromal

* Corresponding author. The Wallace H. Coulter Department of Biomedical Engineering, Georgia Institute of Technology and Emory University, Atlanta, GA, 30332, USA.
E-mail address: krish.roy@gatech.edu (K. Roy).
[1] These authors contributed equally to the manuscript.

https://doi.org/10.1016/j.biomaterials.2021.120683
Received 25 September 2020; Received in revised form 4 January 2021; Accepted 14 January 2021
Available online 25 January 2021

cells [9–11]. Across these distinct microenvironments, stromal cells, including osteoblasts, stromal cells, endothelial cells, CXCL12-abundant reticular (CAR) cells, adipocytes, macrophages, and osteocytes, have all been implicated in regulating HSC fate [12–14]. As HSCs differentiate, hematopoietic progenitor cells (HPCs) occupy distinct microenvironments within the BM, where they differentiate into lymphoid and myeloid lineages [15].

The ability to replicate the juxtaposition and interaction of the endosteal and perivascular niches is important to understand the complexity of the human BM niche (Fig. 1A). The endosteal niche is primarily constituted of osteoblasts (OBs) and osteoclasts [12]. OBs express ECM in the endosteal microenvironment (e.g., collagen I, fibronectin, and osteopontin). OBs also provide soluble and surface bound signals, like Jagged-1 and stem cell factor (SCF), to HSCs and HPCs that regulate differentiation and potency. The endosteal niche was believed to be relatively hypoxic and this was thought to promote HSC maintenance of potency; however, recent studies have found that the endosteal niche could be less hypoxic [16], in part, due to vascularization throughout the bone compartment. BM sinusoids permeate the bone cavity and serve as the connection between BM and peripheral tissues, allowing for the egress of progenitors of the hematopoietic system [17]. Endothelial cells (ECs) comprise the BM sinusoids and are accompanied by mesenchymal stromal cells (MSCs) or pericytes in establishing the perivascular niche. Abundant levels of stromal derived factor 1 (SDF1 or CXCL12) and SCF are expressed in the perivascular space to establish the HSC niche and recent *in vivo* studies have observed HSCs to be resident in the perivascular niche [18–20].

The BM HSC niche has been a subject of study for decades and there have been many efforts to recapitulate aspects of the niche *in vitro*. Various material approaches and simple co-culture platforms in both 2D and 3D have been reported to increase HSC proliferation or maintain HSC potency during *in vitro* culture [21–24]. Culture systems have also been developed that mimic specific cytokine [25] or ECM [26] environments that HSCs experience in the BM niche *in vivo*. More recently, *ex vivo* and *in vitro* microfluidic or on-chip devices have been designed for recreating the bone or BM microenvironment [27–31]. These studies have recapitulated many characteristics of the bone marrow; however, they either require several weeks of ectopic implantation in animal

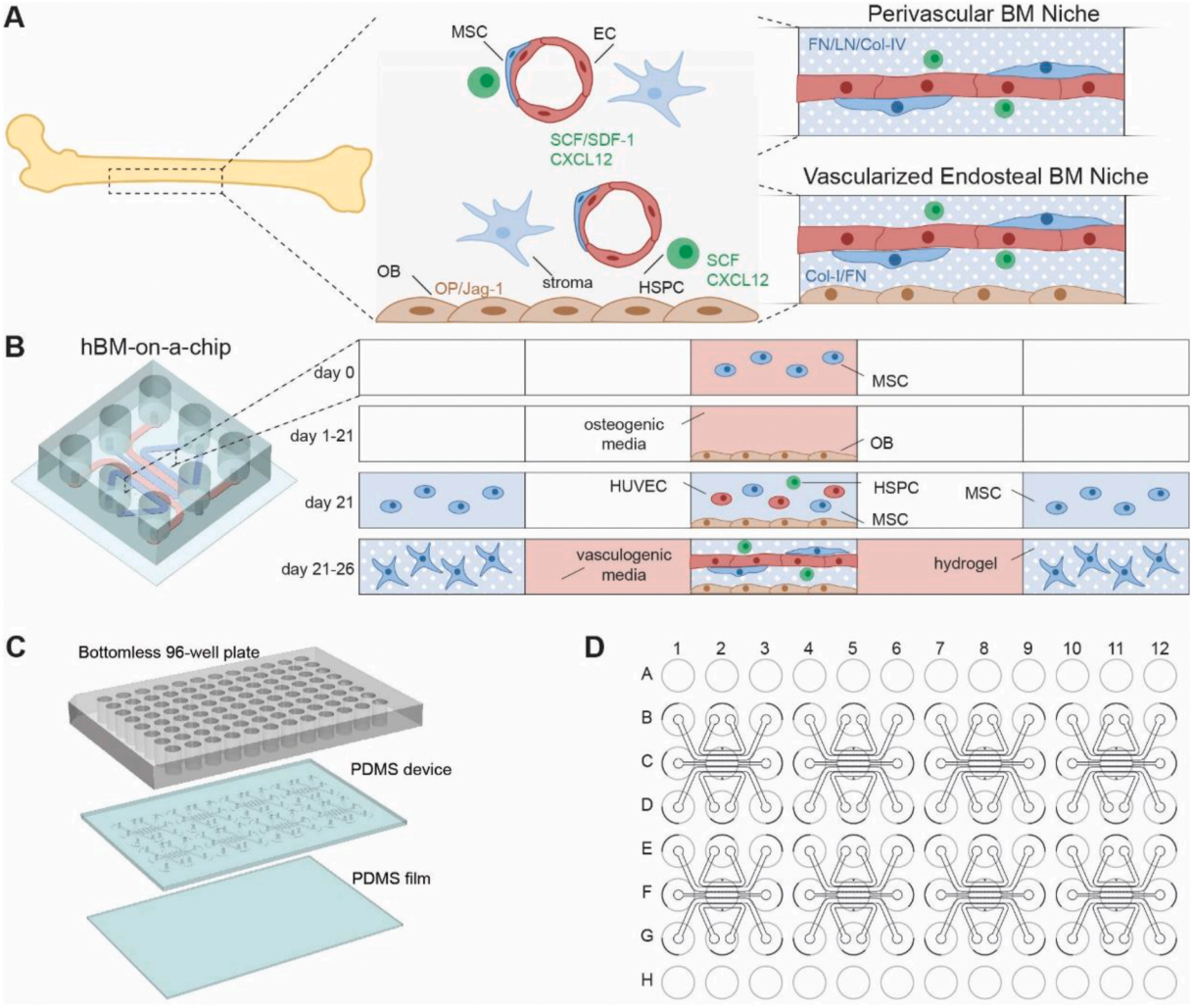

Fig. 1. Schematic of human bone marrow-on-a-chip (hBM-on-a-chip). (A) The hBM-on-a-chip can recapitulate both the central perivascular BM niche (without OBs) and the vascularized endosteal BM niche (with OBs) that are found in the cavities of long bones. MSC = mesenchymal or marrow stromal cells, including pericytes; OB = osteoblasts and mineralized bone-like tissue layer; stromal cells = other cells of the BM stroma including CXCL12-abundant reticular cells (CAR), matured hematopoietic cells, and adipose cells. Note the area between vasculatures represent the central marrow region. FN = Fibronectin; LN = Laminin, Col I and IV = Collagen I and Collagen IV; OP = Osteopontin; Jag-1 = Jagged 1. (B) A 5-channel PDMS microfluidic device was fabricated using standard soft lithography techniques. MSCs are first differentiated for 21 days in the central channel of the device to form an endosteal layer, then HUVECs, MSCs, and HSPCs are loaded on top of the endosteal layer and vasculogenesis occurs over 5 days to form the hBM-on-a-chip. (C) 3D assembly of 96-well plate schematic of hBM-on-a-chip. (D) 96-well plate layout of hBM-on-a-chip.

models, do not recreate the 3D microvasculature of the BM, or do not incorporate interactions between the multiple juxtaposed niches (endosteal, perivascular and central marrow) of the hBM microenvironment. While others have developed microcavity arrays to study the hBM microenvironment, they also have not been used to specifically study the endosteal niche or its interactions with the spatially-juxtaposed niches [32–34]. Therefore, there is an unmet need for developing microphysiological mimics of the human bone marrow microenvironment consisting of the multiple niches and study how the various niches impact HSC behavior under physiological or pathological conditions.

Here, we present development and evaluation of a multi-niche microfluidic human BM-on-a-chip (hBM-on-a-chip) in a 96-well plate high-throughput format. Each plate has eight independent BM devices consisting of a human MSC-derived endosteal surface overlaid with a 3D microvascular hydrogel network representing the central marrow and perivascular niches of the hBM (Fig. 1B).

We demonstrate characterization and application of this device to study hematopoietic stem and progenitor cell (HSPC) behavior, and response to pathological stimulus, such as radiation. Specifically, we show that the presence or absence of a bone-like surface (endosteal niche) differentially affects HSPCs. Our results indicate that this multi-niche device can be used to study the microphysiological characteristics and responses of human BM physiology, and disease pathologies.

2. Materials and methods

Device design and fabrication. A unique 5-channel microfluidic device was fabricated in a 4 × 2 array to create the BM-Chip, the design of which is described in the Results section. Details of the fabrication protocol are provided in the Supplementary section. To mitigate the risk of devices leaking and failing over the course of their extended culture in a humidified incubator, the finished plates were thoroughly cleaned with 70% EtOH, then DI H_2O, and finally dried at 65 °C overnight.

To promote cell adhesion, the central channel of each device was coated with 0.01% dopamine HCl (Sigma-Aldrich) in TE Buffer [pH 8.5] for 1 h at room temperature, washed with PBS, coated with 100 μg/mL rat tail collagen I (Corning) in PBS for 1 h at room temperature, washed with PBS, and then dried overnight at 65 °C [35]. Plates were sterilized by UV exposure for at least 30 min prior to the culture of cells.

Cell culture. Bone marrow derived human mesenchymal stem cells (MSCs) (RoosterBio) were initially expanded in hMSC-High-Performance-Media (RoosterBio) for one passage. For subsequent passages, MSCs were expanded in αMEM (Sigma-Aldrich) supplemented with 10% FBS (HyClone) and 1% penicillin-streptomycin (HyClone). MSCs were used for culture in devices up to passage 6. Human umbilical vein endothelial cells (HUVECs) (Lonza) were expanded in EGM-2MV (Lonza) on tissue culture flasks coated with 0.1% gelatin (Sigma-Aldrich) and used up to passage 8. Human BM $CD34^+$ cells (Lonza) were expanded for 5 days in Stemline II (Sigma-Aldrich) supplemented with 100 ng/mL SCF, TPO, and G-CSF (Peprotech). All cells were cultured at 37 °C and 5% CO_2.

Osteogenesis in hBM-on-a-chip. MSCs were seeded within the central channels of devices at a density of 5×10^5 cells/mL. To induce osteogenesis and mineralization, cells were cultured within the devices for 21 days in αMEM osteogenic media (10% FBS, 1% penicillin-streptomycin, 10 mM β-glycerophosphate (Sigma-Aldrich), 50 μM ascorbic acid (Sigma-Aldrich), and 100 nM dexamethasone (Sigma-Aldrich)) with daily media exchange.

Vasculogenesis in hBM-on-a-chip. Vasculogenesis, in the presence or absence of the endosteal, was achieved inside the central channel using a 5 day co-culture of HUVECs and MSCs inside a fibrin-collagen hydrogel [36–38] with media supplemented with VEGF and Angiopoietin-1. The detailed protocol is provided in the supplementary methods.

$CD34^+$ HSPC culture in hBM-on-a-chip. Human BM $CD34^+$ HSPCs were labeled with PKH67 green fluorescent cell stain (Sigma-Aldrich) and mixed with the HUVECs and MSCs, to be loaded at a final concentration of 3×10^5 (20:1 HUVEC:HSPC ratio, 6×10^5 HSPCs/mL in thrombin cell suspension prior to mixing with fibrinogen). This concentration results in ~500 HSPCs within the central channel of each device. Devices were imaged on days 1, 3, and 5 after loading, using a Lionheart-FX, and analyzed using the Gen5 (BioTek Instruments) software.

Radiation exposure. On day 5, hBM-on-a-chip plates were transported to an animal facility and exposed to ionizing radiation using an RS 2000 X-ray Irradiator (Rad Source). To control for effects of transportation, untreated samples were also transported to the facility. The duration of the process (transportation to and from the facility and X-ray exposure) was ~1 h, during which time the samples were not held at 37 °C, 5% CO_2.

3. Results

The 96-well format multi-niche hBM-on-a-Chip enables robust, higher throughput co-culture of human BM-niche cells. The bone marrow microenvironment contains multiple spatially-distinct niches (Fig. 1A). In order to culture multiple cell types in the same device and create complex yet integrated niches, the design needed to (A) enable the extended culture and differentiation of progenitor cells into the endosteal niche, and (B) allow for loading of the perivascular and central marrow cells and hydrogel precursors into a previously wetted channel. To mitigate these key technical challenges, we designed a five-channel device, consisting of one central "gel channel", two media channels, and two outer gel channels (Fig. 1B). The device was based on some recently published methods [39,40], with key modifications that promoted maintenance of the air-liquid interface between the cell-containing central channel and adjacent media channels during the initial phase of culturing the endosteal niche. Briefly, the channel height was set to 150 μm, the communication pores between the gel channels were narrowed to 50 μm in width, and the number of communication pores was limited to decrease media leakage from the central channel during osteogenesis. The theoretical difference between advancing pressure and burst pressure (see supplementary methods) was calculated to be 28.5 cm H_2O, allowing for efficient loading of fluid into the device.

To improve on the design and standardization of the hBM-on-a-chip, a 4 × 2 array of 5-channel devices was integrated into standard well-plates. Using published methods [38,41–43], the PDMS "device" layer was bonded directly to a bottomless 96-well plate (Fig. 1C and D). The resulting array of 8 devices uses the wells of the 96-well plate as media reservoirs and as a window for imaging the central channel of the device (Figure S1F). This creates an eight-device array on each plate, with consistent, known, orientation which not only provides an n = 8 per plate configuration for improved reproducibility, but also makes the platform readily compatible with automated imaging systems, or potentially, high-throughput media handling instrumentation. In subsequent analyses, the term "device" refers to a single unit on the 8-device-containing "plate" or hBM-on-a-chip.

On-Chip osteogenic differentiation of MSCs create a mineralized endosteum-like niche. Polydopamine (PDA) and collagen I coating [35] on the central-channel PDMS surface improved MSC attachment, compared to collagen I or fibronectin (Figure S2A). MSCs seeded at a high density on the coated central-channel and differentiated in osteogenic media showed increased mineralization over 21 days, as observed by Alizarin red (Fig. 2A and B) and von Kossa (Fig. 2C and D) staining. At day 21, 71 ± 18% of the device-area stained positive for Alizarin red with a normalized mean intensity of 0.64 ± 0.07; while 91 ± 3% of the device-area stained positive for von Kossa with normalized mean intensity of 0.60 ± 0.06. In addition, this mineralized, surrogate endosteal niche, expressed key endosteum-associated cytokines like SCF, SDF1 also known as CXCL12, the notch-ligand Jagged-1, as well as

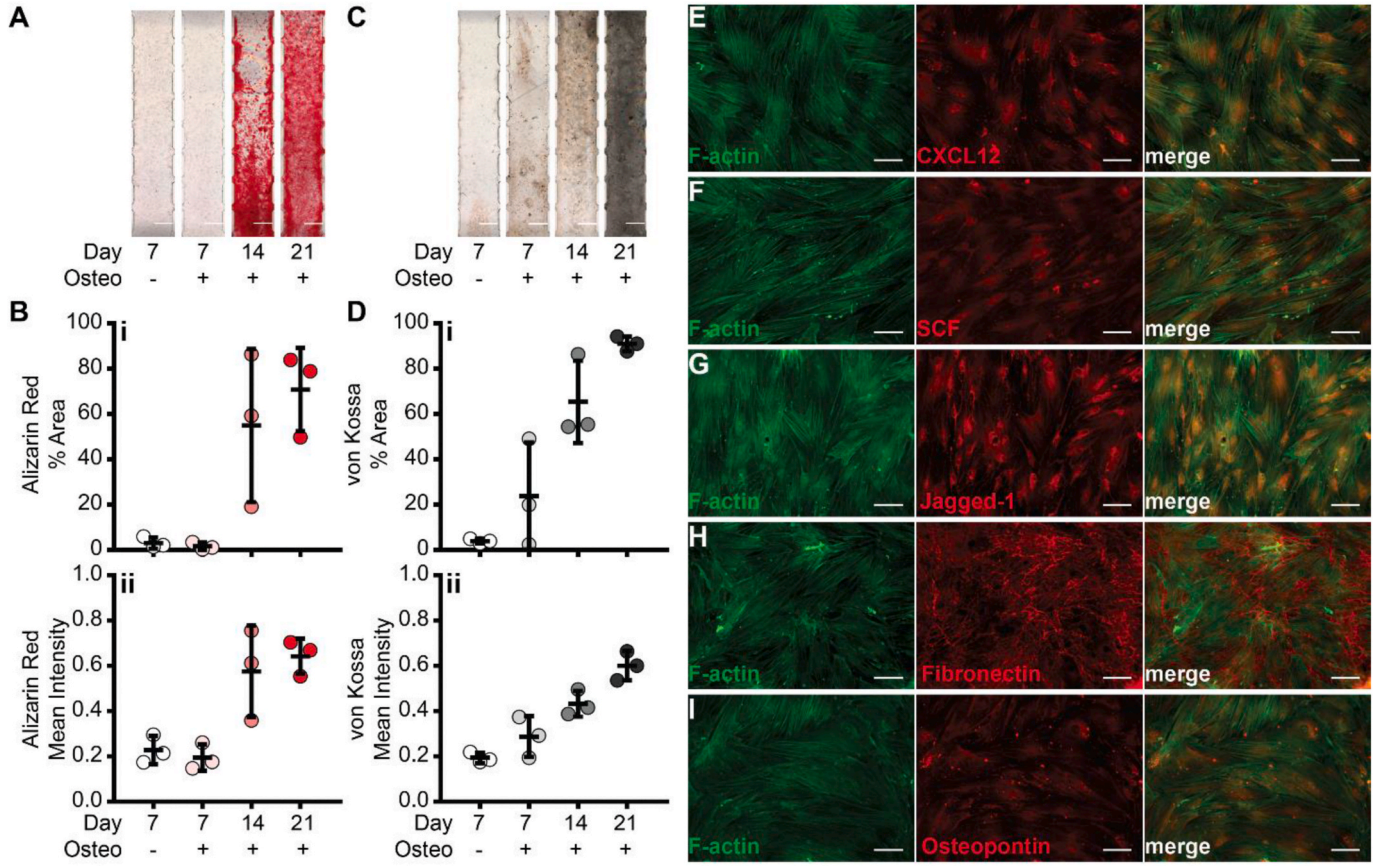

Fig. 2. Formation of the endosteal niche. MSCs were differentiated for 21 days within the central channel of the hBM-on-a-chip after which mineralization was measured. Representative images of (A) alizarin red and (C) von Kossa staining. Scale bars: 500 μm. Quantification of (B) alizarin red and (D) von Kossa staining by (i) percent area and (ii) mean intensity. Data are plotted as mean ± SD (n = 3 devices). Immunofluorescence staining of endosteal cytokines (E) CXCL12, (F) SCF, and (G) Jagged-1. Immunofluorescence staining of endosteal ECM (H) fibronectin, and (I) osteopontin, was observed using immunofluorescence staining. Scale bars: 100 μm. (For interpretation of the references to colour in this figure legend, the reader is referred to the Web version of this article.)

physiologically relevant ECM components like fibronectin and osteopontin – indicating that in-vivo like biomolecular characteristics of the human BM endosteum can be achieved (Fig. 2E–I).

MSC and endothelial cell co-culture in Fibrin-Collagen hydrogel allows robust generation of the central marrow and perivascular niches on top of the endosteal niche. Amongst various methods for *in vitro* vasculogenesis in microfluidic devices [37,39,40,44] we found that vasculature formation and perfusion was most consistent using a combination of MSCs in laterally adjacent channels (same cells used to generate the endosteum), supplementation with VEGF and Angiopoietin-1 (ANG-1), and encapsulation of human umbilical vein endothelial cells (HUVECs) in the fibrin/collagen hydrogel (Figure S3).

To understand the role of stromal cells and the endosteal niche on vasculogenesis and cytokine secretion, hBM-on-a-chip devices were created with and without the central marrow MSCs, and/or the endosteal layer (OBs) (Fig. 3A). We observed no significant difference in either total vascular-area with MSCs (41.4 ± 4.4%), OBs (44.1 ± 2.9%), or both cell types (44.3 ± 3.1%) present, when compared to EC-only devices (43.39 ± 3.3%) (Fig. 3B). Similarly, the total network-lengths were also similar (MSCs 83.0 ± 13.0 mm, OBs 92.9 ± 12.2 mm, MSCs + OBs 92.1 ± 10.8 mm, or EC-only 83.3 ± 6.2 mm) (Fig. 3C). Similar analyses on average diameter and junction density were also found to have no significant differences among groups (Figure S6A-B).

On day 5 of vasculogenesis (Fig. 3D), culture-media from the devices were analyzed for secreted cytokines. In general, OB containing devices secreted higher amounts of cytokines. IL-6, a cytokine involved in B cell differentiation, was highly expressed in EC + OB (624 ± 212 pg/mL) and EC + MSC + OB (386 ± 49 pg/mL) samples, compared to in EC (162 ± 49 pg/mL) and EC + MSC (132 ± 34 pg/mL) devices. IL-11, responsible for signaling during megakaryocyte maturation, was low or negligible in EC (4.1 ± 1.8 pg/mL) and EC + MSC device-media, while substantially present in EC + OB (308 ± 73 pg/mL) and EC + MSC + OB (254 ± 64 pg/mL) devices. Similarly, M-CSF, which induces macrophage differentiation of HSCs, was elevated in EC + OB (58.3 ± 5.3 pg/mL) and EC + MSC + OB (68.6 ± 2.1 pg/mL) devices, compared to EC (15.2 ± 7.6 pg/mL) and EC + MSC (10.3 ± 3.5 pg/mL) devices. Relatively small concentrations of IL-7 (reported to promote lymphoid progenitor differentiation), IL-34 (differentiation of monocytes and macrophages), GM-CSF (differentiation of granulocytes and macrophages), FLT-3L (differentiation of dendritic cells), and SCF (HSC maintenance) were also measured, and there were no significant differences across groups. Amounts of secreted CXCL12 (hematopoietic chemoattractant) and IL-3 (myeloid progenitors) present in the media, were below detection limits.

After 5 days of vasculogenesis, the devices were fixed and stained to characterize the presence and localization of cytokines and ECM (Fig. 3E–G, Figure S6C-D). Both CXCL12 and SCF were found to be expressed by the perivascular and the endothelial cells. Fibronectin was present in the "central marrow" space outside of the vasculature. These spatial distributions of cytokines are consistent with their reported *in vivo* distributions [45].

The endosteal niche reduced expansion of HSPCs in hBM-on-a-chip, but increased maintenance of CD34 expression. We then investigated how human $CD34^+$ BM-HSPCs expand in the hBM-on-a-chip and how MSCs and OBs affected their fate. We measured expansion via microscopy over the 5 days of vasculogenesis (Fig. 4A and

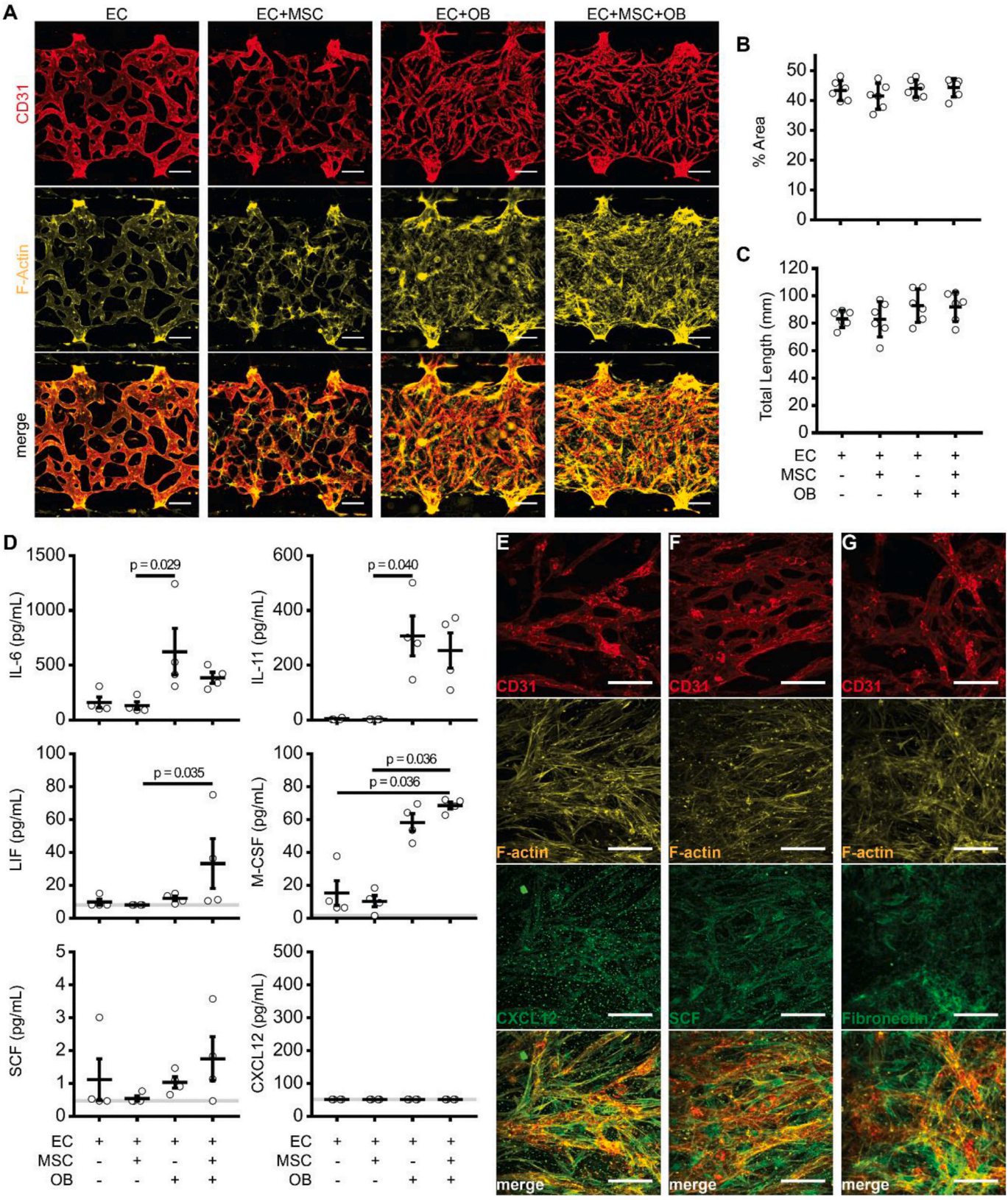

Fig. 3. Vasculogenesis and cytokine expression in hBM-on-a-chip. hBM-on-a-chip with or without MSCs and OBs created using a fibrin (4 mg/mL) and collagen I (1 mg/mL) co-gel with VEGF (50 ng/mL, days 1–5) and Ang-1 (100 ng/mL, days 3–5) supplementation. (A) Immunofluorescence staining of CD31 (red) and F-actin (yellow). Scale bars: 100 μm. Quantification of the (B) percent area and (C) total length of vascular networks. Data are plotted as mean ± SD (n = 4–6 devices). Data were analyzed using a one-way ANOVA with Tukey's post hoc test. No significance found at $p < 0.05$. (D) Hematopoietic cytokine secretion measured in device supernatant collected on day 5. Data are plotted as mean ± SEM (n = 4 devices). Data were analyzed using Kruskal-Wallis w/Dunn's post hoc test. Significance between groups ($p < 0.05$) is indicated in the figure. Immunofluorescence staining of (E) CXCL12, (F), SCF, (G) fibronectin after 5 days vasculogenesis in EC + MSC + OB hBM-on-a-chip. Scale bars: 100 μm. (For interpretation of the references to colour in this figure legend, the reader is referred to the Web version of this article.)

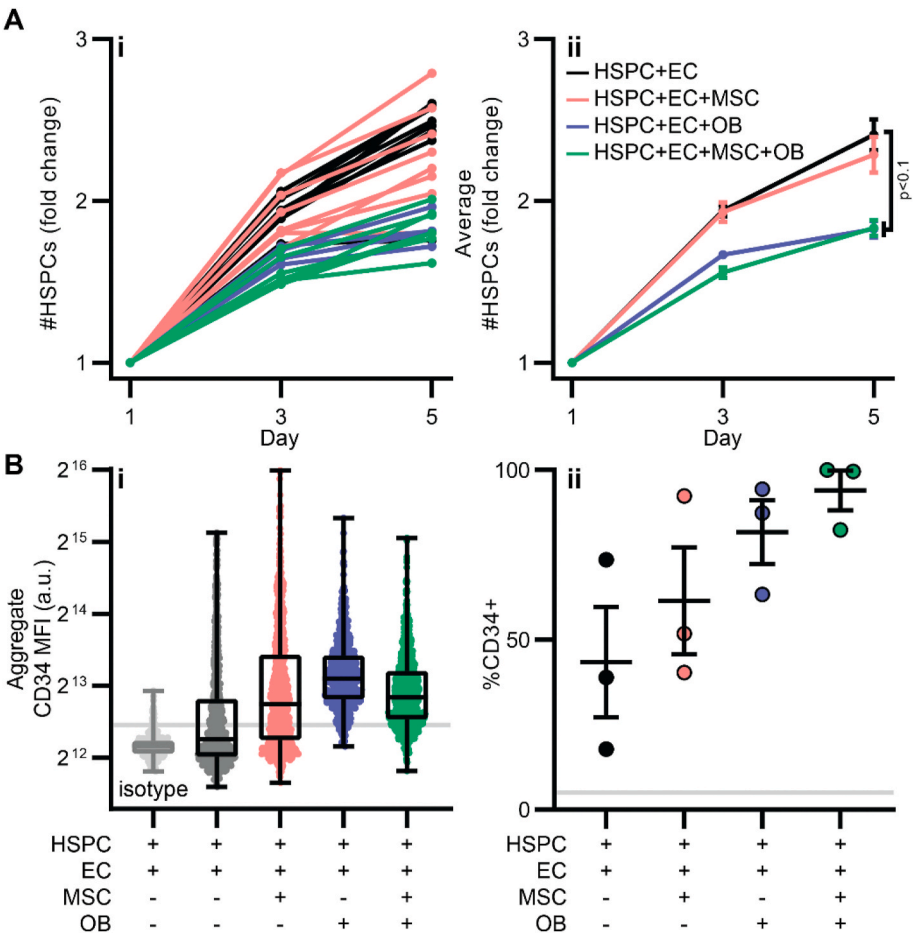

Fig. 4. CD34$^+$ HSPC behavior in hBM-on-a-chip. (A) Fold change number of HSPCs ((i) individual devices and (ii) summary data) on days 1, 3, and 5. Data are shown as mean ± SEM. (n = 4 devices EC + OB, n = 7 devices EC + MSC + OB, n = 8 devices EC and EC + MSC). Data were analyzed using Kruskal-Wallis w/ Dunn's multiple comparisons test. EC vs EC + OB p = 0.0813; EC vs EC + MSC + OB p = 0.0162. (B) Quantification of immunofluorescence of HSPCs cultured for 5 days in hBM-on-a-chip with ECs only (black), with MSCs (red), OBs (blue), and both (green). (i) Aggregate MFI of CD34. Data are shown with median, quartiles, min and max (n = 452 cells for isotype from 1 device, n = 799–907 cells for experimental groups pooled from 3 devices). (ii) Percentage of CD34$^+$ cells. Data are shown as mean ± SEM (n = 3 devices). Grey line is percentage of CD34$^+$ cells in isotype sample using gating scheme. (For interpretation of the references to colour in this figure legend, the reader is referred to the Web version of this article.)

Figure S4A). On day 1, the number of HSPCs in hBM-on-a-chip was not significantly different in MSC and/or OB containing devices. By day 3 and continuing to day 5, devices without OBs had significantly more HSPCs (2.28–2.41-fold expansion) than devices with the endosteal layer (1.83-fold expansion) (Fig. 4Aii).

We also measured the effect of MSCs and OBs on the maintenance of HSPC stemness in the hBM-on-a-chip by monitoring surface expression of CD34 and CD38 by immunohistochemistry. HSPCs were pre-labeled with PKH67 (Figure S4B) and stained for CD34 at Day 5. Devices with MSCs and/or OBs had a higher percentage of CD34$^+$ HSPCs and more CD34 expression on the HSPCs (Fig. 4B). Across the groups, CD38 expression by HSPCs was not detected above the isotype control (Figure S4C).

The endosteal niche reduced apoptosis of HSPCs from exposure to ionizing radiation (IR). To investigate the effect of ionizing radiation on the BM microenvironment, after 5 days of vasculogenesis, hBM-on-a-chip containing OBs, MSCs, and ECs were exposed to 0 Gy or 5 Gy X-ray irradiation. Device supernatants were collected at 0 h (pre-treatment) and 24 h post-exposure. To measure radiation-induced cellular toxicity, the change in lactate dehydrogenase (LDH) activity in the culture-media after irradiation was measured (Figure S5C). The LDH activity in devices exposed to 5 Gy X-ray radiation increased on average, after exposure, while the activity in devices exposed to 0 Gy radiation slightly decreased during the same period, although the difference between the two groups were not statistically significant. The changes in various cytokines, secreted by the hBM-niche after radiation, were also measured and IL-6, IL-7, IL-11, M-CSF, and SCF were found to be lower, on average, in the irradiated group, with some cytokines experiencing a significant decrease (Fig. 5D).

We further investigated whether the endosteal niche is more protective to ionizing radiation for HSPCs. hBM-on-a-chip with (EC + MSC + OB + HSPC) and without (EC + MSC + HSPC) the endosteal niche, were exposed to 5 Gy X-ray radiation and apoptosis-induced DNA fragmentation was measured 24 h after exposure via a terminal deoxynucleotidyl transferase-mediated dUTP-biotin nick-end labelling (TUNEL) assay, counterstained with CD45 (Fig. 5). Although some background of apoptotic HSPCs was observed in non-radiated devices (Fig. 5B and C), we observed a significant increase in TUNEL$^+$ HSPCs in -OB devices (22.6 ± 1.9%, p = 0.052), but no change in +OB devices exposed to 5 Gy radiation (17.7 ± 2.0%). This suggests the endosteal niche provides protection to HSPCs from radiation damage.

4. Discussion

Recently, multiple groups have significantly advanced our understanding of BM physiology and pathologies. For example, a recent study used single-cell and spatial transcriptomics to map the molecular and cellular compositions of various BM niches in the mouse [5]. Another previous study used intravital imaging to elucidate key physiological properties of the BM [17]. These were important investigations but were performed using mouse models due to obvious limitations of using these technologies to study the human BM. To address this issue, several groups have made significant progress in developing *ex vivo* and *in vitro* models of the human BM to ask specific questions that are difficult to study *in vivo*. For example, the Ingber group reported several years ago a BM-chip model that incorporated an endothelial monolayer juxtaposed with a central marrow-like niche. Recently they used this device to successfully model key human disease physiologies [27,31,46]. Other groups have also reported macroscale models based on tissue-engineering principles, primarily for maximizing HSC expansion

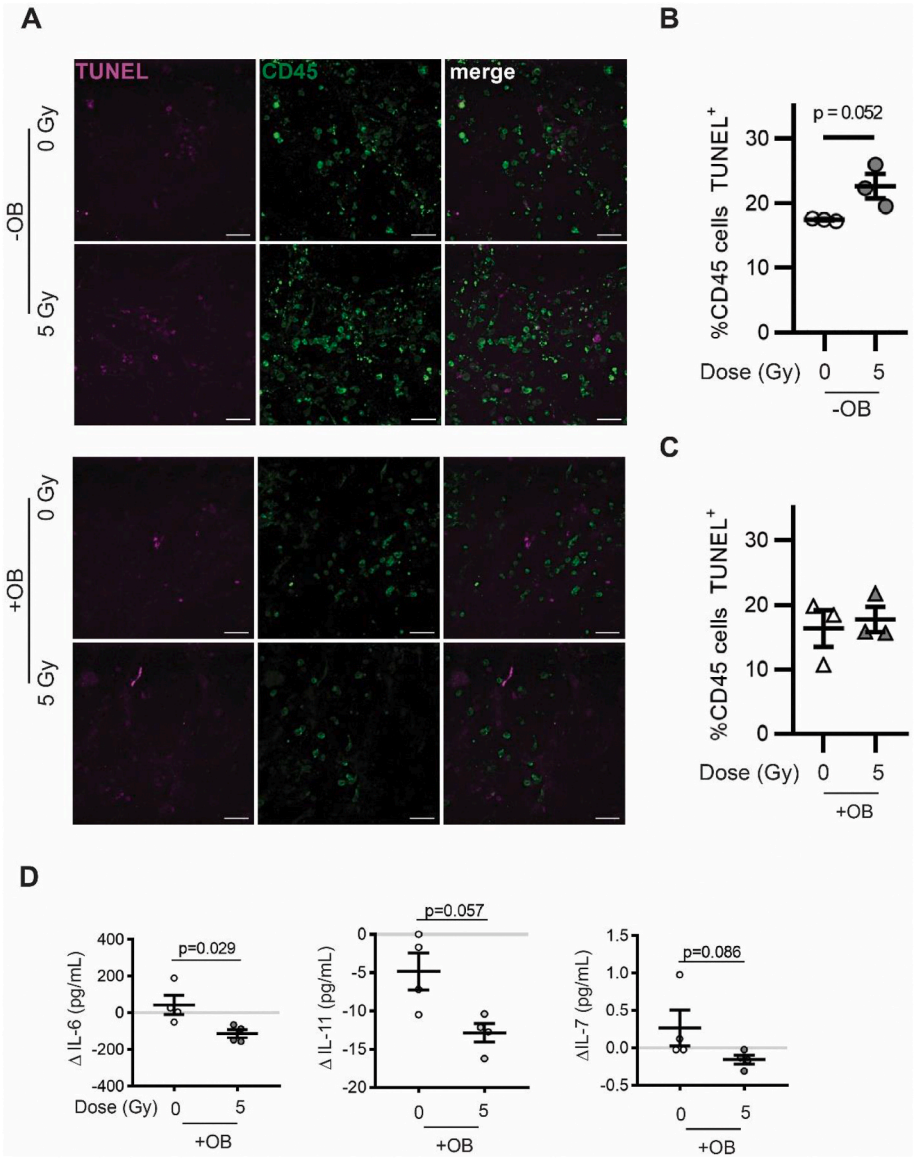

Fig. 5. Effect of endosteal niche on ionizing radiation damage to HSPCs. (A) Representative images of TUNEL (magenta) and CD45 (green) staining of devices, with (bottom panels) or without (upper panels) OBs, exposed to 0 or 5 Gy radiation 24 h after exposure. Scale bar: 50 μm. (B) Quantification of percentage of TUNEL$^+$ CD45 cells, without OBs, 24 h after 0 (white) or 5 (grey) Gy. (C) Quantification of percentage of TUNEL$^+$ CD45 cells, with OBs, 24 h after 0 (white) or 5 (grey) Gy. Data are shown as mean ± SEM (n = 3 devices, with each data point being the percentage of TUNEL + cells out of 131–286 CD45$^+$ cells within 5 ROIs in the device). Data analyzed using student's t-test. (D) Change in hematopoietic cytokines measured in hBM-on-a-chip (EC + MSC + OB) supernatant before (0 h) and 24 h after devices were exposed to 0 or 5 Gy X-ray radiation. Data are shown as mean ± SEM (n = 4 devices). Data analyzed using Mann-Whitney *U* test. (For interpretation of the references to colour in this figure legend, the reader is referred to the Web version of this article.)

[6,24,30].

Despite these major progresses, microphysiological models of the human BM that incorporates the endosteal-like niche along with the central-marrow and a 3D interconnected microvascular niche, similar to that found in the *in vivo* BM environment, have not been developed. Our goal here was to make key technological advances that allows us to fabricate such a complex multi-niche device and study the specific role of the endosteal niche in the human BM and how it affects hBM physiology and pathology. By inclusion of multiple spatially-distinct niches encapsulated in physiologically-relevant biomaterials, we demonstrate that inclusion of the endosteal niche significantly affects the hBM-chip microenvironment, HSC proliferation, fate, as well as HSC-damage after radiation exposure. We believe this on-chip platform would be a useful tool for studying human BM physiology, HSC biology and hematopoiesis, cancer metastasis into the BM, various BM diseases including myelomas and radiation-induced BM failures, and for the screening of therapeutics that target or affect the human BM.

Our 96-well plate-based design evolved from previous iterations that were fabricated entirely out of PDMS. Although fully-PDMS-based devices are free from any geometric constraints [47], unlike our device in which the inlet and outlet ports need to correspond to wells of a culture plate, these limitations do not prevent us from culturing physiologically-relevant models of the human BM. Not only is our hBM-chip capable of culturing multiple niches in a spatially distinct manner, but the 96-well plate format allows for higher-throughput and more reproducible devices and enables the automated collection and analysis of data. An additional unexpected benefit of moving to this fabrication method was the increase in yield of viable of devices during the 21-day differentiation of MSCs, compared to the earlier all-PDMS iterations of the design. The PDMS portion of the construct is sandwiched between a rigid polystyrene frame and a glass coverslip. Thus, the devices are always handled via the plastic well plate and never handled by the channel-bearing PDMS portion, which minimizes small deformations during handling. This resulted in a much lower frequency (less than 5%) of device "failure" (Figure S2B-D). These devices can robustly maintain the extended air-liquid interface required in our model of the hBM microenvironment.

The hBM-chip was capable of expressing key markers of the *in vivo* endosteal niche within the simplified, microfluidic model. Although the day 0 MSCs were seeded on a Collagen I-coated surface, by the end of culture, we were able to detect robust ECM and mineral deposition (Fig. 2), suggesting that the cells were secreting their own ECM proteins to remodel their surroundings into a better hBM-mimic. Osteoblasts are well-known to directly interact with HSCs, potentially through the

expression of Jagged-1, which interacts with Notch on the surfaces of HSCs, to enable HSC maintenance [12]. The MSC-derived endosteal niche of our device, express Jagged-1 on their surface (Fig. 2G) and seem to reduce HSC proliferation, while maintaining CD34 expression (Fig. 4), indicating that the hBM-chip is able to model HSC maintenance in the endosteum. The OBs also secreted physiologically-relevant cytokines, providing further support that we have successfully created a physiologically-relevant human HSPC niche on a chip.

Although our results demonstrate the need for the inclusion of an endosteal niche to accurately model HSPC behavior *in vitro*, it also includes the perivascular stroma in which HSPCs are known to reside [19]. Importantly, the hBM-chip enabled the formation of a 3D microvasculature above the endosteal niche, which is a more physiologically-relevant model of the *in vivo* microenvironment. Furthermore, the device-design permits the detection of key biomolecules both through surface marker staining as well as through analyses of the flow-through media. Although this model did not include adipose and adipose-derived cells and other stromal cells [5], it was still capable of producing detectable levels of key cytokines of the BM niche, such as IL-6, M-CSF, and LIF, especially in the presence of the endosteal niche (Fig. 3D) [15], indicating that OBs may also play a significant role in shaping of the cytokine milieu of the hBM.

A key finding of our hBM-chip was that CXCL12 was expressed abundantly on cell surfaces, but not detectable on the flow-through media (Figs. 2 and 3). CAR-cells (CXCL12-abundant reticular cells) are critically important for BM homeostasis and plays a major role in various BM function. We found that our endosteal niche (OB cells) expresses CXCL12 (indicating presence of CAR-OB cells, Fig. 2) and in the complete device, CXCL12 staining can be found in many perivascular microniches (Fig. 3) – similar to what the recent single cell and spatial transcriptomic work has shown for the mouse BM [5]. Since CXCL12 is secreted and then bound and presented by the ECM, it is expected that we would see CXCL12 in the extracellular space (Fig. 3E, Figure S6C-D) and not so much in the media.

The inclusion of multiple niches within the device, particularly the inclusion of the endosteal niche, also resulted in a more physiologically-relevant behavior of HSPCs within the device, in that they proliferated while maintaining CD34 expression with low or no CD38 expression. We plan to continue the characterization of the HSPCs without the device by performing colony forming cell (CFC) or long term culture initiating cell (LTC-IC) assays to measure the specific subpopulations of progenitors that arise within the BM-chip. While CFC and LTC-IC assays could give more details about individual progenitor populations within the devices, they would require the pooling of HSPCs from multiple devices in order to harvest enough cells to perform a robust assay. Therefore, we believe that the imaging and media sampling studies demonstrated here underscore the power of this microfluidic device to provide key insights into HSPC proliferation and maintenance without the need for labor-intensive standard HSPC assays. It is important to underscore that the purpose of this device was not to maximize HSC proliferation for production [24], but rather to study the homeostatic maintenance of HSCs in the BM and to better understand HSC physiology in more *in vivo* like conditions – as such we did not optimize conditions to maximize HSC proliferation.

In order to demonstrate the utility of our device as a proxy for modeling various failures of the bone marrow, we chose to study the effects of ionizing radiation. IR results in the depletion of hematopoietic cells, causes a range of hematopoietic pathologies, and can cause fatality. Unexpectedly, exposure to relatively high doses of X-ray radiation did not induce significant increase in cell death in our hBM-on-a-chip (EC + MSC + OB). While the impacts of IR on the hematopoietic system are well characterized [48,49], the corresponding effects on the HSPC and BM niches are less understood. MSCs are resistant to the effects of IR and might provide protection to other radiation-damaged cells [50]. Osteoblast activity is downregulated [51–53], decreasing the deposition of endosteal matrix and possibly, in conjunction with upregulation of osteoclasts, causing loss of bone mass [54]. We observed a trend of decreased cytokine expression 24 h after radiation exposure. This suggests that the BM-niche was altered without widespread apoptosis of stromal cells. HSPCs cultured in the vascularized endosteal niche (HSPC + EC + MSC + OB) did not exhibit a significant increase in apoptosis 24 h after exposure. In comparison, we observed a significant increase in $TUNEL^+$ HSPCs in the perivascular niche (HSPC + EC + MSC, no OB) after 5 Gy radiation exposure. Our model suggests that MSC-derived osteoblasts, i.e., the endosteal OB niche, may be similarly radio-protective to HSPC. Further study measuring the production of reactive oxygen species (ROS) after radiation exposure of the perivascular and vascularized endosteal niches may help explain the difference in HSPC outcome in these microenvironments.

5. Conclusion

In summary, we have demonstrated that a multi-niche, microfluidic, microvascular human bone marrow on a chip device can be reproducibly fabricated and can recapitulate key physiological properties of the human BM microenvironment. This platform could be used to study a variety of human BM physiologies and pathologies, including preclinical applications in cancer metastasis, multiple myelomas, and bone marrow failure syndromes.

This manuscript reports a 96-well format, high-throughput, fully-human microfluidic system that represents a physiologically relevant microtissue model of the human bone marrow (hBM). The hBM-on-a-chip incorporates all three primary niches – a bone-like endosteal niche, a stromal-cell containing central marrow niche, and a 3D interconnected network of microvasculature as the perivascular niche. The model recapitulates key features of the hBM, including physiological biomolecular expressions and CD34 cell maintenance; and provides key insights on the role of the endosteal niche on hBM hemostasis and radiation-induced pathologies.

Author contributions

M.R.N. designed and performed experiments, analyzed data, and wrote the manuscript. D. G analyzed data and wrote the manuscript. J.C. M., D.F.R., and E.K. performed experiments, analyzed data, and edited the manuscript. K.R. designed experiments and edited the manuscript.

Declaration of competing interest

The authors declare that they have no known competing financial interests or personal relationships that could have appeared to influence the work reported in this paper.

Acknowledgments

We would like to acknowledge the Georgia Tech Parker H. Petit Institute Core Facilities for their services and shared resources that enabled us to produce this publication. This research was supported by funding from the Georgia TechFoundation (to K.R.), Georgia Tech Research Alliance (to K.R.), the Marcus foundation (to K.R.), NSF Engineering Research Center for Cell Manufacturing Technologies (CMaT) (NSF Grant EEC 1648035 to K.R.), and NSF Graduate Research Fellowship under Grant No. DGE-1148903 (to M.R.N., D.G. and J.C.M.). Parts of this work were performed at the Georgia Tech Institute for Electronics and Nanotechnology, a member of the National Nanotechnology Coordinated Infrastructure (NNCI), which is supported by the National Science Foundation (ECCS-2025462).

Appendix A. Supplementary data

Supplementary data to this article can be found online at https://doi.org/10.1016/j.biomaterials.2021.120683.

References

[1] V.W. Yu, D.T. Scadden, Hematopoietic stem cell and its bone marrow niche, Curr. Top. Dev. Biol. 118 (2016) 21–44, https://doi.org/10.1016/bs.ctdb.2016.01.009.

[2] S.J. Morrison, D.T. Scadden, The bone marrow niche for haematopoietic stem cells, Nature 505 (2014) 327–334, https://doi.org/10.1038/nature12984.

[3] M. Hines, L. Nielsen, J. Cooper-White, The hematopoietic stem cell niche: what are we trying to replicate? J. Chem. Technol. Biotechnol. 82 (2008) 1115–1121, https://doi.org/10.1002/jctb.

[4] A. Wilson, A. Trumpp, Bone-marrow haematopoietic-stem-cell niches, Nat. Rev. Immunol. 6 (2006) 93–106, https://doi.org/10.1038/nri1779.

[5] C. Baccin, et al., Combined single-cell and spatial transcriptomics reveal the molecular, cellular and spatial bone marrow niche organization, Nat. Cell Biol. 22 (2020) 38–48, https://doi.org/10.1038/s41556-019-0439-6.

[6] P.E. Bourgine, I. Martin, T. Schroeder, Engineering human bone marrow proxies, Cell Stem Cell 22 (2018) 298–301, https://doi.org/10.1016/j.stem.2018.01.002.

[7] L.M. Calvi, et al., Osteoblastic cells regulate the haematopoietic stem cell niche, Nature 425 (2003) 841–846, https://doi.org/10.1038/nature02040.

[8] J. Zhang, et al., Identification of the haematopoietic stem cell niche and control of the niche size, Nature 425 (2003) 836–841, https://doi.org/10.1038/nature02041.

[9] M.J. Kiel, S.J. Morrison, Maintaining hematopoietic stem cells in the vascular niche, Immunity 25 (2006) 862–864, https://doi.org/10.1016/j.immuni.2006.11.005.

[10] L. Ding, T.L. Saunders, G. Enikolopov, S.J. Morrison, Endothelial and perivascular cells maintain haematopoietic stem cells, Nature 481 (2012) 457–462, https://doi.org/10.1038/nature10783.

[11] J.Y. Chen, et al., Hoxb5 marks long-term haematopoietic stem cells and reveals a homogenous perivascular niche, Nature 530 (2016) 223–227, https://doi.org/10.1038/nature16943.

[12] S.L. Ellis, S.K. Nilsson, The location and cellular composition of the hemopoietic stem cell niche, Cytotherapy 14 (2012) 135–143, https://doi.org/10.3109/14653249.2011.630729.

[13] Y. Omatsu, et al., The essential functions of adipo-osteogenic progenitors as the hematopoietic stem and progenitor cell niche, Immunity 33 (2010) 387–399, https://doi.org/10.1016/j.immuni.2010.08.017.

[14] S. Mendez-Ferrer, et al., Mesenchymal and haematopoietic stem cells form a unique bone marrow niche, Nature 466 (2010) 829–834, https://doi.org/10.1038/nature09262.

[15] L. Ding, S.J. Morrison, Haematopoietic stem cells and early lymphoid progenitors occupy distinct bone marrow niches, Nature 495 (2013) 231–235, https://doi.org/10.1038/nature11885.

[16] J.A. Spencer, et al., Direct measurement of local oxygen concentration in the bone marrow of live animals, Nature 508 (2014) 269–273, https://doi.org/10.1038/nature13034.

[17] S. Upadhaya, et al., Intravital imaging reveals motility of adult hematopoietic stem cells in the bone marrow niche, Cell Stem Cell (2020), https://doi.org/10.1016/j.stem.2020.06.003.

[18] Y. Kunisaki, et al., Arteriolar niches maintain haematopoietic stem cell quiescence, Nature 502 (2013) 637–643, https://doi.org/10.1038/nature12612.

[19] M. Acar, et al., Deep imaging of bone marrow shows non-dividing stem cells are mainly perisinusoidal, Nature 526 (2015) 126.

[20] T. Itkin, et al., Distinct bone marrow blood vessels differentially regulate haematopoiesis, Nature 532 (2016) 323, https://doi.org/10.1038/nature17624. https://www.nature.com/articles/nature17624#supplementary-information.

[21] M.R. Nelson, K. Roy, Bone-marrow mimicking biomaterial niches for studying hematopoietic stem and progenitor cells, J. Mater. Chem. B 4 (2016) 3490–3503, https://doi.org/10.1039/c5tb02644j.

[22] Lutolf, M. P., Gilbert Pm Fau - Blau, H. M. & Blau, H. M. Designing Materials to Direct Stem-Cell Fate.

[23] J.S. Choi, B.P. Mahadik, B.A. Harley, Engineering the hematopoietic stem cell niche: frontiers in biomaterial science, Biotechnol. J. 10 (2015) 1529–1545, https://doi.org/10.1002/biot.201400758.

[24] P.E. Bourgine, et al., In vitro biomimetic engineering of a human hematopoietic niche with functional properties, Proc. Natl. Acad. Sci. U. S. A. 115 (2018) E5688–E5695, https://doi.org/10.1073/pnas.1805440115.

[25] B.P. Mahadik, S. Pedron Haba, L.J. Skertich, B.A.C. Harley, The use of covalently immobilized stem cell factor to selectively affect hematopoietic stem cell activity within a gelatin hydrogel, Biomaterials 67 (2015) 297–307, https://doi.org/10.1016/j.biomaterials.2015.07.042.

[26] L. Jansen, T. McCarthy, M. Lee, S. Peyton, A synthetic, three-dimensional bone marrow hydrogel, bioRxiv (2018), https://doi.org/10.1101/275842, 275842.

[27] Y.S. Torisawa, et al., Bone marrow-on-a-chip replicates hematopoietic niche physiology in vitro, Nat. Methods 11 (2014) 663–669, https://doi.org/10.1038/nmeth.2938.

[28] B.M. Holzapfel, et al., Tissue engineered humanized bone supports human hematopoiesis in vivo, Biomaterials 61 (2015) 103–114, https://doi.org/10.1016/j.biomaterials.2015.04.057.

[29] A. Marturano-Kruik, et al., Human bone perivascular niche-on-a-chip for studying metastatic colonization, Proc. Natl. Acad. Sci. U. S. A. 115 (2018) 1256–1261, https://doi.org/10.1073/pnas.1714282115.

[30] M.V.J. Braham, et al., A human hematopoietic niche model supporting hematopoietic stem and progenitor cells in vitro, Adv Healthc Mater 8 (2019), e1801444, https://doi.org/10.1002/adhm.201801444.

[31] D.B. Chou, et al., On-chip recapitulation of clinical bone marrow toxicities and patient-specific pathophysiology, Nat Biomed Eng (2020), https://doi.org/10.1038/s41551-019-0495-z.

[32] P. Wuchter, et al., Microcavity arrays as an in vitro model system of the bone marrow niche for hematopoietic stem cells, Cell Tissue Res. 364 (2016) 573–584, https://doi.org/10.1007/s00441-015-2348-8.

[33] I. Kurth, K. Franke, T. Pompe, M. Bornhauser, C. Werner, Extracellular matrix functionalized microcavities to control hematopoietic stem and progenitor cell fate, Macromol. Biosci. 11 (2011) 739–747, https://doi.org/10.1002/mabi.201000432.

[34] M.P. Lutolf, R. Doyonnas, K. Havenstrite, K. Koleckar, H.M. Blau, Perturbation of single hematopoietic stem cell fates in artificial niches, Integr Biol (Camb) 1 (2009) 59–69, https://doi.org/10.1039/b815718a.

[35] Y.J. Chuah, et al., Simple surface engineering of polydimethylsiloxane with polydopamine for stabilized mesenchymal stem cell adhesion and multipotency, Sci. Rep. 5 (2015) 18162, https://doi.org/10.1038/srep18162.

[36] J.S. Jeon, et al., Human 3D vascularized organotypic microfluidic assays to study breast cancer cell extravasation, Proc. Natl. Acad. Sci. U. S. A. 112 (2015) 214–219, https://doi.org/10.1073/pnas.1417115112.

[37] J.S. Jeon, et al., Generation of 3D functional microvascular networks with human mesenchymal stem cells in microfluidic systems, Integr Biol (Camb) 6 (2014) 555–563, https://doi.org/10.1039/c3ib40267c.

[38] J.C. Mejias, M.R. Nelson, O. Liseth, K. Roy, A 96-well format microvascularized human lung-on-a-chip platform for microphysiological modeling of fibrotic diseases, Lab Chip (2020), https://doi.org/10.1039/D0LC00644K.

[39] M.B. Chen, et al., On-chip human microvasculature assay for visualization and quantitation of tumor cell extravasation dynamics, Nat. Protoc. 12 (2017) 865.

[40] S. Oh, et al., Open-top" microfluidic device for in vitro three-dimensional capillary beds, Lab Chip 17 (2017) 3405–3414, https://doi.org/10.1039/c7lc00646b.

[41] D.T.T. Phan, et al., A vascularized and perfused organ-on-a-chip platform for large-scale drug screening applications, Lab Chip 17 (2017) 511–520, https://doi.org/10.1039/c6lc01422d.

[42] S.P. Desai, D.M. Freeman, J. Voldman, Plastic masters-rigid templates for soft lithography, Lab Chip 9 (2009) 1631–1637, https://doi.org/10.1039/b822081f.

[43] W. Wu, J. Wu, J.H. Kim, N.Y. Lee, Instantaneous room temperature bonding of a wide range of non-silicon substrates with poly(dimethylsiloxane) (PDMS) elastomer mediated by a mercaptosilane, Lab Chip 15 (2015) 2819–2825, https://doi.org/10.1039/c5lc00285k.

[44] X.L. Wang, et al., Engineering anastomosis between living capillary networks and endothelial cell-lined microfluidic channels, Lab Chip 16 (2016) 282–290, https://doi.org/10.1039/c5lc01050k.

[45] S.K. Nilsson, et al., Immunofluorescence characterization of key extracellular matrix proteins in murine bone marrow in situ, J. Histochem. Cytochem. 46 (1998) 371–377.

[46] Y.S. Torisawa, et al., Modeling hematopoiesis and responses to radiation countermeasures in a bone marrow-on-a-chip, Tissue Eng. C Methods 22 (2016) 509–515, https://doi.org/10.1089/ten.TEC.2015.0507.

[47] R. Visone, et al., A simple vacuum-based microfluidic technique to establish high-throughput organs-on-chip and 3D cell cultures at the microscale, Advanced Materials Technologies 4 (2019) 1800319, https://doi.org/10.1002/admt.201800319.

[48] M.H. Barcellos-Hoff, C. Park, E.G. Wright, Radiation and the microenvironment - tumorigenesis and therapy, Nat. Rev. Canc. 5 (2005) 867–875, https://doi.org/10.1038/nrc1735.

[49] T.M. Fliedner, D. Graessle, C. Paulsen, K. Reimers, Structure and function of bone marrow hemopoiesis: mechanisms of response to ionizing radiation exposure, Cancer Biother. Radiopharm. 17 (2002) 405–426, https://doi.org/10.1089/108497802760363204.

[50] T. Sugrue, N.F. Lowndes, R. Ceredig, Mesenchymal stromal cells: radio-resistant members of the bone marrow, Immunol. Cell Biol. 91 (2013) 5–11, https://doi.org/10.1038/icb.2012.61.

[51] J.S. Greenberger, M. Epperly, Bone marrow-derived stem cells and radiation response, Semin. Radiat. Oncol. 19 (2009) 133–139, https://doi.org/10.1016/j.semradonc.2008.11.006.

[52] M. Dominici, et al., Restoration and reversible expansion of the osteoblastic hematopoietic stem cell niche after marrow radioablation, Blood 114 (2009) 2333–2343, https://doi.org/10.1182/blood-2008-10-183459.

[53] X. Cao, et al., Irradiation induces bone injury by damaging bone marrow microenvironment for stem cells, Proc. Natl. Acad. Sci. U. S. A. 108 (2011) 1609–1614, https://doi.org/10.1073/pnas.1015350108.

[54] D.E. Green, C.T. Rubin, Consequences of irradiation on bone and marrow phenotypes, and its relation to disruption of hematopoietic precursors, Bone 63 (2014) 87–94, https://doi.org/10.1016/j.bone.2014.02.018.